

# Design and Simulation of a Three-Phase Induction Motor Speed Control System

\*<sup>1</sup>Gbenga A. Olarinoye, <sup>2</sup>Mudathir F. Akorede, and <sup>1</sup>Charles D. Akinropo

<sup>1</sup>Department of Electrical Engineering, Ahmadu Bello University Zaria, Kaduna, Nigeria

<sup>2</sup>Department of Electrical and Electronics Engineering, University of Ilorin, Ilorin, Nigeria

oyeguzeh@yahoo.com | akorede@unilorin.edu.ng | akinropocharles@gmail.com

## ORIGINAL RESEARCH ARTICLE

Received: 12-DEC-2021; Reviewed: 13-JAN-2022; Accepted: 13-MAR-2021

<http://dx.doi.org/10.46792/fuoyejt.v7i1.735>

**Abstract-** Three-phase Induction motors are increasingly used in a variety of applications such as fans, milling machines, transportation, etc. In applications requiring precise speed control such as robotics, centrifugal pumps, mills and other high-performance applications, it is essential that speed is maintained constant at a desired fixed value. Many speed control techniques exist in literature but this paper presents the design of a simple PI controller and its use to control the speed of a three-phase induction motor. A controller design that applies the Phase margin (PM) as the stability criterion is employed. The cross-over frequency and phase margin of the open loop gain of motor and controller are specified in order to develop a stable control system. The three-phase induction motor model is presented and modified for the purpose of control. A comparative analysis between the motor performance with and without the PI controller was performed. The unit step response of the speed control loop is characterized by rise time, settling time, steady state error and peak overshoot of 0.0253s, 0.19s, 2.22e-14% and 24.03% respectively. Simulation results show that the speed of the uncontrolled motor changed whereas that of the controlled motor returned quickly to its initial value after the motor is subjected to load disturbances in steady state.

**Keywords-** Controller, Induction motor, Model, Speed control, Steady state.

## 1 INTRODUCTION

Induction motors are widely acclaimed to be the work horses of the industry owing to their robustness, low cost, ruggedness and ease of speed control (Mosbah and El-Zhori, 2019; Magagula, Nnachi and Akumu, 2020; Li *et al.*, 2021; Sahu, Mohanty and Mishra, 2021). Applications of Induction motors include but not limited to variable speed drives such as electric vehicles, trains, ships (Kousalya and Singh, 2021) and multi-speed drive systems such as in washing machines, rolling mills and centrifugal pumps. Induction motors are traditionally designed to operate in applications where motor speed does not change frequently because it is difficult to control motor speed (Biswal and Satpathy, 2021).

It is difficult to control speed because the flux and torque in the induction motor are coupled i.e., they are not independently controlled as in the case of the direct current (DC) motors in which the torque and flux producing components are independent of each other (Biswal and Satpathy, 2021). The advent of power electronic converters and fast digital signal processors now makes it easier to control induction motor speed (Richardson, Patterson and Parchment, 2021; Jafari, *et al.*, 2021; Alahmad and Kaçar, 2021). Instead of driving the induction motor directly from the AC mains, it can now be driven from power converters that are capable of varying the magnitude, frequency and phase angle of the voltage applied to the motor according to certain control algorithms in order to bring about a desired change in torque and hence speed of the motor (Abad, 2017; Umar, Akbar and Kazmi, 2018; Hareesh and Jayanand, 2021).

Many speed control strategies have therefore been developed over the last two decades that take advantage of advances in semiconductor technologies, pulse width modulation techniques and control algorithms (Richardson *et al.*, 2021; Sahu, Mohanty and Mishra, 2021; Zand *et al.*, 2021). The result manifests in the increasing areas of applications for the existing induction motors. Many applications exist in which it is required to maintain motor speed at a precise value no matter the changes in the load. Other applications require the motor to be driven at varying or multiple speeds in order to improve the process output (Umar, Akbar and Kazmi, 2018).

In Mosbah and El-Zhori (2019), the use of Atmega 328/p with PI controller for speed control of a three-phase inverter-fed induction motor was presented. The standard three phase induction motor model was applied. Simulation results obtained in MATLAB/Simulink showed different rise time, percentage speed overshoot and very minimal steady state speed error values for three different pulse width modulation techniques. In Metwaly *et al.* (2019), an induction motor fed from three phase PWM ac chopper was presented. The control strategy involves an outer speed control loop and an inner current control loop. A PI controller that regulates the magnitude of the supply reference current in order to achieve input power factor correction of the drive system. The control strategy depends on changing only the stator voltage. The *d-q* reference frame model of the induction motor was also used in the work. While it is simple, the strategy works for a limited speed range.

Lim *et al.* (2018) proposed an advanced control strategy involving a speed controller and a slip controller for a five-leg voltage source inverter that drives a dual three phase induction motor. The slip controller maintains the mechanical speed of the two motors equal regardless of any load changes. A rotor flux-oriented control method

\*Corresponding Author

Section B- ELECTRICAL/ COMPUTER ENGINEERING & RELATED SCIENCES

Can be cited as:

Olarinoye G.A., Akorede M.F., and Akinropo C.D. (2022): Design and Simulation of a Three-Phase Induction Motor Speed Control System, *FUOYE Journal of Engineering and Technology* (FUOYEJET), 7(1), 39-46. <http://dx.doi.org/10.46792/fuoyejt.v7i1.735>

was applied for the speed control. Both controllers are PI controllers but the design for the controllers was not given much attention. Maximum control speed was limited by the limitation imposed on the DC link voltage.

Ke *et al.* (2020) proposed a low constant speed control strategy for heavy haul electric locomotives, utilizing a 3-phase induction motor, based on a variable PI regulator. An indirect stator-quantities control was used to modulate the space voltage vector for the purpose of achieving a low constant speed. A luenberger observer model was used to calculate actual motor speed and a variable PI controller was employed to adjust speed error in order to output the desired torque. Samudera *et al.*, (2020) implemented a PI and IP controller in MATLAB to regulate the induction motor speed during load changes. They utilized a space vector PWM technique and a scalar control strategy to drive the motor and maintain its speed whenever there is a change in load.

While most of these papers have sought to demonstrate the performances of converter structures, PWM schemes and the possibility of achieving higher and/or cleaner output voltage, the methodology of the determination of controller gains for speed regulation has not been given adequate attention. This paper seeks to address this issue. Its aim is to first, re-model the three-phase induction motor in a way that decouples the torque from the flux in the motor via a vector control technique and second, to apply a single proportional plus integral (PI) controller to improve the dynamic response and regulate motor speed at the desired value. The paper demonstrates the design of the PI controller by specifying a desired bandwidth and phase margin and then using the conditions of high stability margins to calculate the controller gains. This paper will show that the PI controller ensures a fast and stable closed loop speed control. The rest of the paper is organized into sections. Section 2 describes the three-phase induction motor model and a modification of it to allow for independent control of torque and flux in the motor. Section 3 deals with the methodology of speed control and the controller design while Section 4 provides the results and discussion. The conclusion is provided in Section 5.

**2 MATHEMATICAL MODEL**

In modelling the three-phase induction motor, the three phase windings of the stator and rotor are usually represented by equivalent orthogonal set of *d-q* axis windings which produce the same MMF in the airgap. The schematic diagram of a line-operated three-phase induction motor is illustrated in Figure 1. Its equivalent in *d - q* coordinates is drawn in Figure 2. The *a-b-c* phase winding voltages  $V_{as}$ ,  $V_{bs}$  and  $V_{cs}$  are first transformed to their equivalent *d-q* winding voltages,  $V_{ds}$  and  $V_{qs}$  in order to analyze motor operation. The *d-q* reference frame model of the three-phase induction motor is provided in equations (1)-(10) (Krause *et al.*, 2013; Metwaly *et al.*, 2019). They are the voltage, flux linkage and torque equations of the three-phase induction motor (Sharma, Parashar and Chandel, 2020).

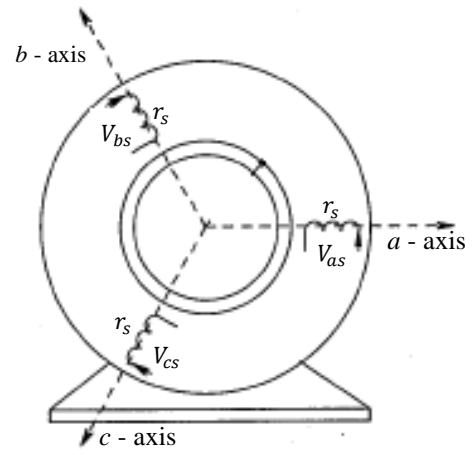


Fig. 1: Three-phase Induction Motor model

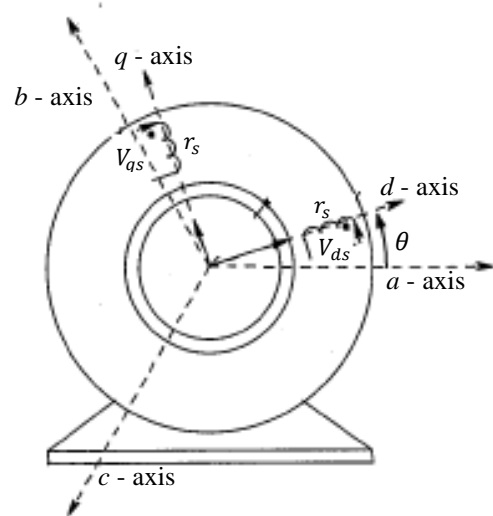


Fig. 2: *d - q* Equivalent Model of a three-phase induction motor

$$V_{ds} = R_s i_{ds} + \frac{d}{dt} \lambda_{ds} - \omega_e \lambda_{qs} \tag{1}$$

$$V_{qs} = R_s i_{qs} + \frac{d}{dt} \lambda_{qs} + \omega_e \lambda_{ds} \tag{2}$$

$$V'_{dr} = R_r i'_{dr} + \frac{d}{dt} \lambda'_{dr} - \omega_{sl} \lambda'_{qr} \tag{3}$$

$$V'_{qr} = R_r i'_{qr} + \frac{d}{dt} \lambda'_{qr} + \omega_{sl} \lambda'_{dr} \tag{4}$$

$$\lambda_{ds} = L_s i_{ds} + L_m i'_{dr} \tag{5}$$

$$\lambda_{qs} = L_s i_{qs} + L_m i'_{qr} \tag{6}$$

$$\lambda'_{dr} = L_r i'_{dr} + L_m i_{ds} \tag{7}$$

$$\lambda'_{qr} = L_r i'_{qr} + L_m i_{qs} \tag{8}$$

$$T_e = \frac{3}{2} \left( \frac{p}{2} \right) (\lambda'_{dr} i_{qs} - \lambda'_{qr} i_{ds}) \tag{9}$$

$$pW_m = \frac{T_e - T_L}{J_{eq}} \tag{10}$$

$V_{ds}$ ,  $V_{qs}$ ,  $V'_{dr}$ ,  $V'_{qr}$  are the stator and rotor voltages in the *d-q* synchronous reference frame. Subscript 's' represents stator quantities while subscript 'r' represents rotor

quantities.  $i_{ds}$ ,  $i_{qs}$ ,  $i'_{dr}$  and  $i'_{qr}$  are the stator and rotor currents.  $\lambda_{qs}$ ,  $\lambda_{ds}$ ,  $\lambda'_{dr}$  and  $\lambda'_{qr}$  are the flux linkages in the stator and rotor.  $R_s$  and  $R_r$  are the stator and rotor winding resistances respectively.  $L_m$  is the magnetizing inductance.  $L_s$  is self-inductance of the stator windings while  $L'_r$  is the self-inductance of the rotor windings. Primed quantities are quantities of the rotor referred to the stator.  $\omega_e$  and  $\omega_{sl}$  are the supply and slip angular frequency respectively.  $J_i$  is the inertia of the rotor and the connected load while  $T_l$  is the load torque.  $T_{em}$  is the electromagnetic torque produced in the motor.

### 3 MODIFICATIONS TO THE MODEL

In order to effectively decouple the flux from torque in the motor, the  $d$ -axis is now made to align with the rotor flux linkage space vector as in Figure 3. The Figure illustrates the relationship between the synchronously rotating  $d$ - $q$  reference frame and the stationary reference frame (in which the real machine currents are represented) when the rotor flux vector is properly aligned with the  $d$ -axis. The  $d$ -axis component of this current is seen to be in phase with the rotor flux.

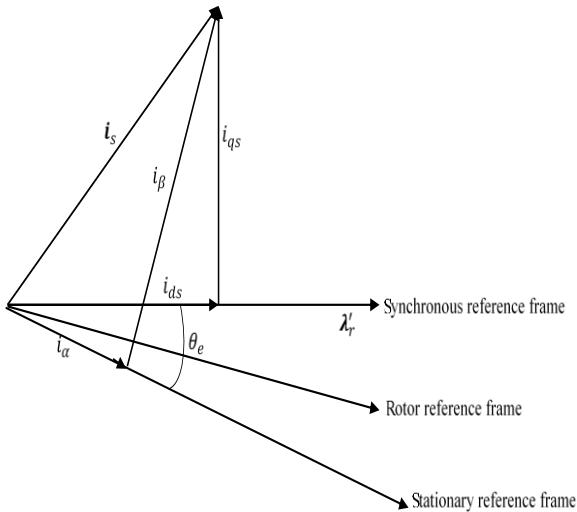


Fig. 3:  $d$ -axis alignment with the rotor flux vector

This means that the  $q$ -axis component of the rotor flux linkage space vector,  $\lambda'_{qr}$  is zero (Umar, Akbar and Kazmi, 2018). The  $d$ -axis component of the rotor flux space vector,  $\lambda'_{dr}$  is now equal to the rotor flux magnitude,  $\lambda_r$ . The rotor flux vector is computed as follows;

$$\lambda_r = \sqrt{\lambda_{qr}^2 + \lambda_{dr}^2} \tag{11}$$

Mathematically, aligning the  $d$ -axis with the rotor flux vector means equating  $\lambda_{qr}$  to zero in equations (3), (4), (8) and (9). Therefore, the following modifications result;

$$\lambda'_r = \lambda'_{dr} \tag{12}$$

$$i'_{qr} = -\frac{L_m}{L'_r} i_{qs} \tag{13}$$

$$\omega_s - \omega_r = \frac{R_r L_m i_{qs}}{L'_r \lambda'_r} \tag{14}$$

With  $i'_{qr}$  substituted as provided in (13), the torque produced in the motor represented by Equation (9) is

modified because of the alignment of the rotor flux magnitude with the  $d$ -axis to the following;

$$T_e = \frac{3P L_m}{2 L'_r} (\lambda'_r i_{qs}) \tag{15}$$

It is important to note that the rotor voltages  $V_{dr}$  and  $V_{qr}$  of the squirrel cage motor are each equal to zero because the rotor windings are short-circuited. This point has been taken into consideration in the modeling. The dynamics of the rotor flux is developed from (3) and (7) to yield;

$$\tau_r \frac{d\lambda'_r}{dt} + \lambda'_r = L_m i_{ds} \tag{16}$$

where  $\tau_r = \frac{L'_r}{R_r}$

The term,  $\tau_r$ , is the rotor circuit time constant. The dependence of the rotor flux on  $i_{ds}$  is evident in Equation (16). The equation describes a first order system with a time constant given by  $\tau_r$ . If the rotor flux,  $\lambda'_r$ , is maintained constant, then according to equation (15) the torque,  $T_e$  will depend entirely on  $i_{qs}$ , which is the component of the stator current in the  $q$ -axis. In this manner, the control of torque and flux may be achieved independently. The modified model which achieves the decoupling of the control of torque and flux in the three-phase induction motor is therefore stated as follows;

$$V_{ds} = R_s i_{ds} + p\lambda_{ds} - \omega_e \lambda_{qs} \tag{17}$$

$$V_{qs} = R_s i_{qs} + p\lambda_{qs} + \omega_e \lambda_{ds} \tag{18}$$

$$\tau_r \frac{d\lambda'_r}{dt} + \lambda'_r = L_m i_{ds} \tag{19}$$

$$\omega_s = \omega_r + \frac{R_r L_m i_{qs}}{L'_r \lambda'_r} \tag{20}$$

$$T_e = \frac{3P L_m}{2 L'_r} (\lambda'_r i_{qs}) \tag{21}$$

$$\lambda_{ds} = L_s i_{ds} + L_m i'_{dr} \tag{22}$$

$$\lambda_{qs} = L_s i_{qs} + L_m i'_{qr} \tag{23}$$

$$\lambda'_r = L'_r i'_{dr} + L_m i_{ds} \tag{24}$$

$$0 = L'_r i'_{qr} + L_m i_{qs} \tag{25}$$

The rotor flux angle is calculated as follows;

$$\theta_e = \int_0^t \omega_e(\tau) d\tau \tag{26}$$

Where  $\tau$  is the variable of integration.  $\theta_e$  is extremely crucial to the realization of the control scheme as its value at every time step is required in order to calculate the command currents that will drive the motor at the desired speed.  $\theta_e$  is also required for the transformation of the  $a$ - $b$ - $c$  currents to their equivalent  $d$ - $q$  values at every time step in accordance to Equations (27) and (28). This action maintains the alignment of the  $d$ -axis with the rotor flux vector. (Abad, 2016).

$$\begin{bmatrix} i_\alpha \\ i_\beta \end{bmatrix} = \frac{2}{3} \begin{bmatrix} 1 & \frac{1}{2} & -\frac{1}{2} \\ 0 & \frac{\sqrt{3}}{2} & -\frac{\sqrt{3}}{2} \end{bmatrix} \begin{bmatrix} i_a \\ i_b \\ i_c \end{bmatrix} \tag{27}$$

$$\begin{bmatrix} i_{ds} \\ i_{qs} \end{bmatrix} = \begin{bmatrix} \cos \theta_e & \sin \theta_e \\ -\sin \theta_e & \cos \theta_e \end{bmatrix} \begin{bmatrix} i_\alpha \\ i_\beta \end{bmatrix} \tag{28}$$

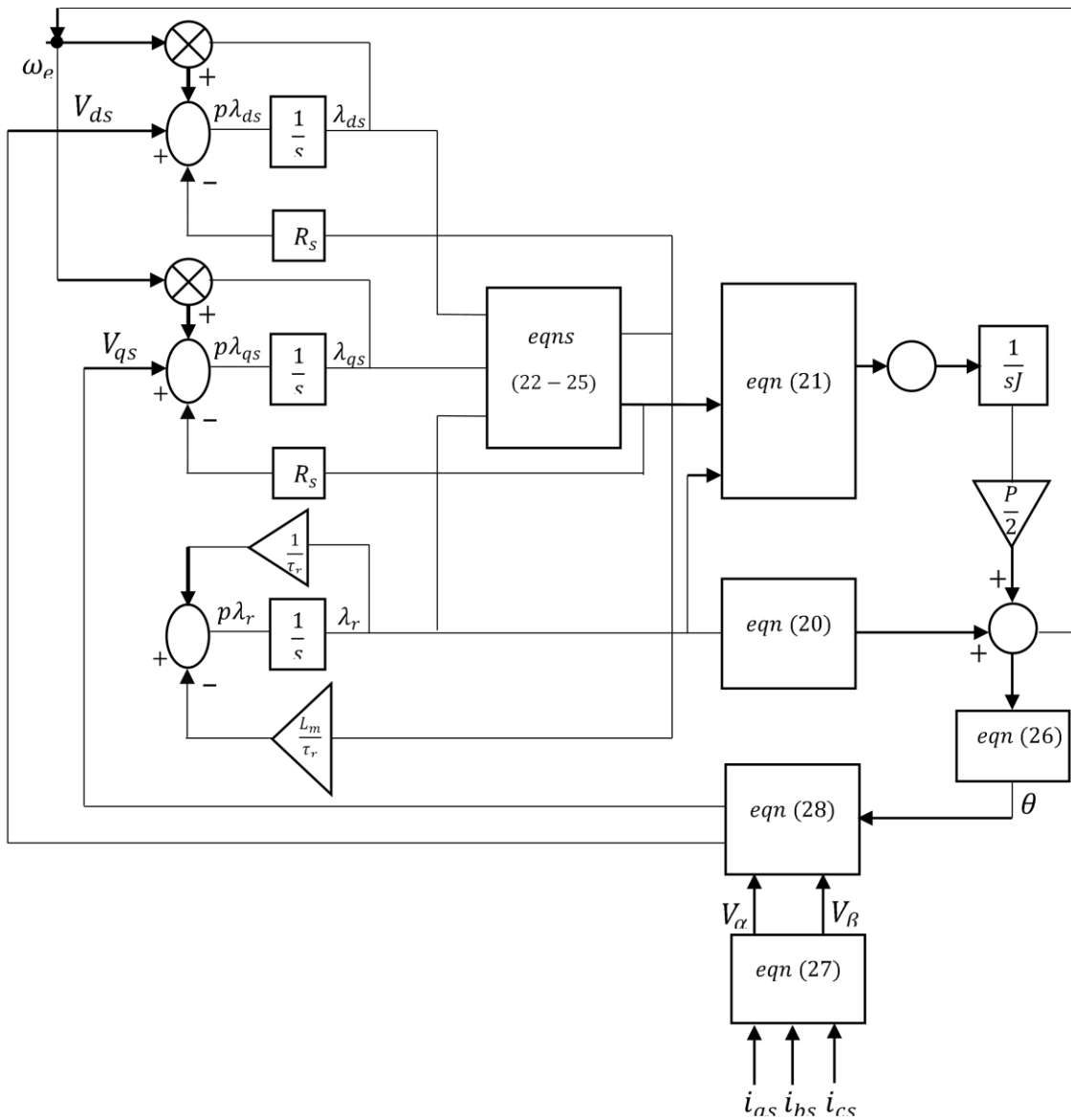


Fig. 4: Block diagram representation of solution to Equations (17) – (28)

The  $d$ - $q$  quantities are constants (or DC values) in balanced sinusoidal steady state and therefore it is easy to design a PI controller for motor speed control. The solution of the model equations (17) – (28) is illustrated in the block diagram of Figure 4. In this Figure, three phase ac currents  $i_{as}$ ,  $i_{bs}$  and  $i_{cs}$  are the inputs to the system while speed is the output. The load torque  $T_L$ , represents the disturbance in the system which may mean a sudden increase or decrease in the applied load. The behaviour of the motor speed when the load is suddenly reduced and increased within its rated value is examined and discussed in section 4.

**4 THE PROPOSED CONTROLLER**

Figure 5 shows the block diagram of the control system of the three-phase induction motor. A current regulated converter is employed to deliver desired current to the three phase-induction motor. The objective of the control design is to make the motor speed constant at rated value regardless of any load disturbances. A simplified

equivalent block diagram of the speed control loop is provided in Figure 6.

The output of the PI block is the DC  $q$ -axis stator current. The relationship is obtained from Equations (21) and (10) with the assumption that  $T_L = 0$ . This current is then transformed to sinusoidal reference motor currents  $i_{abc}^*$  using the inverse transformations of Equations (28) and (27). The reference currents are translated to the motor as command inputs by the converter.

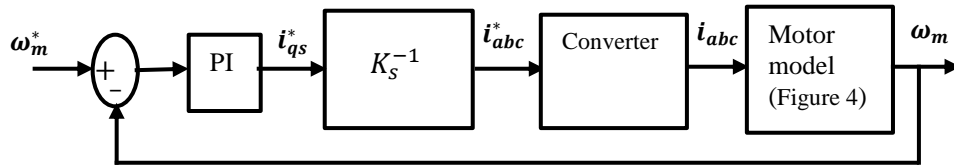


Fig. 5: Speed control loop block diagram

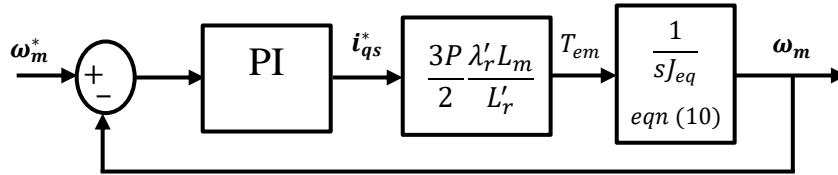


Fig. 6: Simplified block diagram of the speed control loop

where,

$$K_s = \frac{2}{3} \begin{bmatrix} \cos \theta & \sin \theta \\ -\sin \theta & \cos \theta \end{bmatrix} \begin{bmatrix} 1 & \frac{1}{2} & -\frac{1}{2} \\ 0 & \frac{\sqrt{3}}{2} & -\frac{\sqrt{3}}{2} \end{bmatrix} \quad (29)$$

$$PM = 180^\circ + \text{Phase at crossover frequency} \quad (35)$$

Equations (36) and (37) satisfy this condition for the speed control loop.

#### 4.1 CONTROLLER DESIGN

The control system block diagram of Figure 6 is reduced as shown in Figure 7.

$$\left| \frac{k_p(j\omega_c + \frac{k_i}{k_p})c}{-\omega_c^2 J_i} \right| = 1 \quad (36)$$

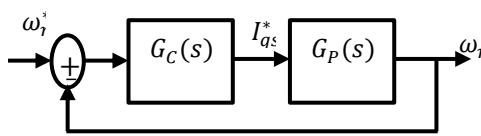


Fig. 7: Reduced speed control loop block diagram

$$PM = \angle \left( \frac{k_p(j\omega_c + \frac{k_i}{k_p})c}{-\omega_c^2 J_i} \right) + 180^\circ \quad (37)$$

where  $\omega_c$  is the crossover frequency of the open loop. The closed loop bandwidth is chosen equal to the crossover frequency and is selected as 50 rad/s so as to obtain a very fast speed response. A phase margin of  $60^\circ$  is chosen for the purpose of achieving a stable closed loop operation. Therefore, the parameters  $k_i$  and  $k_p$  are determined by solving equations (36) and (37) simultaneously. They are derived as closed form solutions provided as follows;

$$G_C(s) = k_p + \frac{k_i}{s} \quad (30)$$

$$G_P(s) = \frac{c}{sJ_{eq}} \quad (31)$$

$G_C(s)$  is the transfer function of the PI controller while  $G_P(s)$  is the transfer function of the motor and the connected load.  $k_p$  and  $k_i$  are the proportional and integral gain respectively.

$$k_i = \frac{J_i \omega_c^2}{k \sqrt{1 + \left(\frac{\omega_c k_p}{k}\right)^2}} \quad (38)$$

$$c = \frac{3P \lambda_r' L_m}{2 L_r'} \quad (32)$$

$$k_p = \frac{\tan(PM)k_i}{\omega_c} \quad (39)$$

$$G_0(s) = G_C(s)G_P(s) = \frac{k_p \left(s + \frac{k_i}{k_p}\right)c}{s^2 J_i} \quad (33)$$

$G_0(s)$  is the open loop gain of the speed control loop. The closed loop gain  $G_{CL}(s)$  can be obtained as follows;

$$G_{CL}(s) = \frac{G_0(s)}{1 + G_0(s)} \quad (34)$$

The key to the design is to avoid a crossover frequency with a phase of  $-180^\circ$ . In other words, a cross-over frequency with a phase of  $-180^\circ$  produces an unstable system. Therefore, to produce a stable speed control system, the chosen cross-over frequency is imposed at a desired phase margin that makes the system stable. The PM must be a positive number such that;

The open loop transfer function is plotted in Figure 8 and it shows a phase margin of  $60^\circ$  at the cross-over frequency of 50 rad/s. The open loop gain plot is above 0 dB and the magnitude rolls off at high frequency. The phase plot does not cross the  $180^\circ$  line. This means that the system has an infinite gain margin (GM) which gives the designer a lot of gain to leverage upon without concerns that the system will become unstable. The closed loop transfer function is plotted in Figure 9. It has a flat shape at 0 dB at low frequency, much like the characteristic of a low pass filter. The phase plot, on the other hand, is  $0^\circ$  at low frequency. These characteristics predict a very close speed reference tracking.

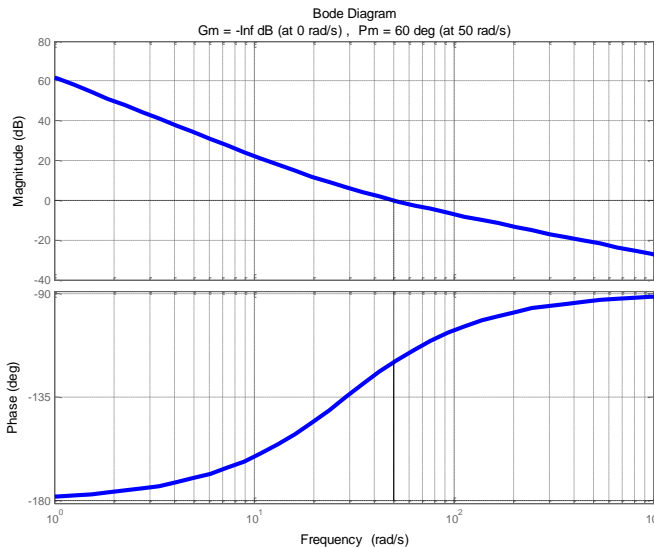


Fig. 8: Open loop frequency response

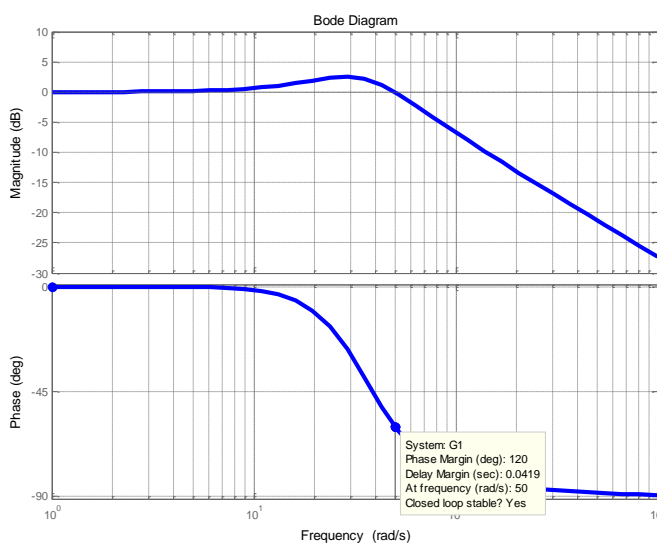


Fig. 9: Closed loop response of the speed control loop

The parameters of the selected three-phase induction motor are provided in Table 1.

Table 1. Parameters of The Three-Phase Induction Motor

Parameters	Values
Rated Power	2.4kW
Line Voltage	460V
Line frequency	60Hz
Rated Speed	1770 rpm
Stator resistance	1.77 $\Omega$
Rotor resistance	1.34 $\Omega$
Stator leakage inductance	0.01392 H
Rotor inductance	0.0126 H
Mutual inductance	0.369 H

## 5 RESULTS AND DISCUSSION

The induction motor was operated in steady state. The load on the motor was suddenly reduced by half from rated value of 1 pu to 0.5 pu and stayed at that value for 1.5s. The load was again reduced by half to 0.25 pu and this load was maintained for a further 1.5s before the load torque was increased to 0.5 pu for an interval of 1s. The load torque was increased further at a time of 4.5s and maintained till the end of simulation time. The decrease and increase in Load torque represent disturbances in the system. The load torque and electromagnetic/induced torque profiles are presented in Figure 10 (a). The speed performance is plotted in Figure 10 (b).

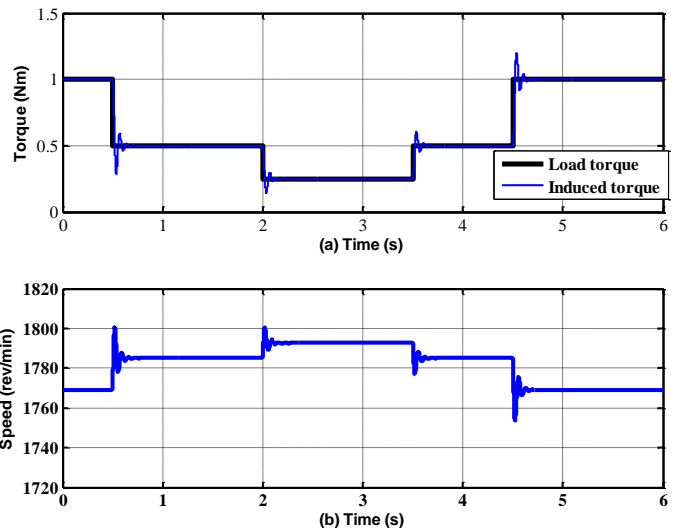


Fig. 10 (a): Load torque and Induced torque (b): Speed performance of the uncontrolled three-phase induction motor

Transients can be observed in the induced torque at the instant of load change in Figure 10 (a). The induced torque is equal to the load torque after the transients die out at steady state. The speed of the motor, on the other hand, rises from its rated value of 1770 rev/min to 1785 rev/min after the change in load from 1 pu to 0.5 pu and then from 1785 rev/min to 1793 rev/min after the reduction in load from 0.5 pu to 0.25 pu. The speed then falls to 1785 rev/min with a rise in load torque at 3.5 s of simulation time. The speed is seen to fall back to the rated value of 1770 rev/min after the rise in load torque back to its rated value. The speed is observed to undergo some transients at the instant of the changes. Oscillations can be seen in the speed as well during these changes.

In an un-controlled system such as this one, speed changes after load disturbances lead to inefficient motor operation. In high performance applications such as robotics and factory automation, speed changes can lead to loss of precision. Neither of these conditions is desirable. Hence the need for speed control. The unit step response of the controlled system is plotted in Figure 11. It can be observed that the step response tracks its reference after a single peak overshoot and a slight undershoot. Associated system performance indices were calculated using the control system tool box in MATLAB and are provided in Table 2.

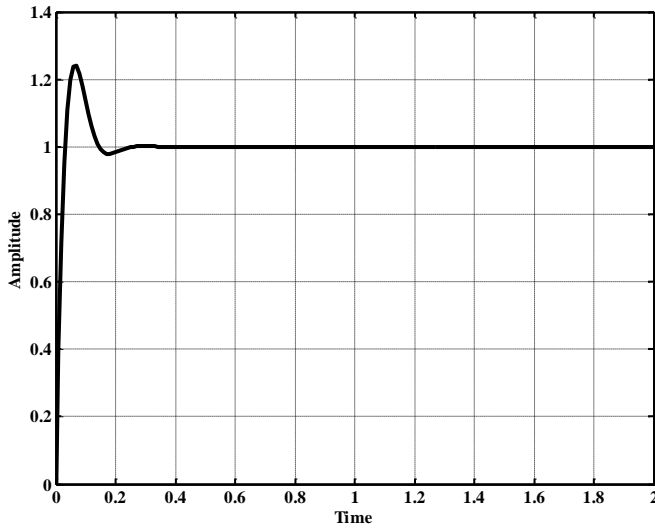


Fig. 11. Unit step response of the speed control loop

Table 2. Command-Tracking Performance of the Speed Control Loop

Performance Index	Value
Rise Time	0.0253s
Maximum Overshoot	24.033%
Peak Time	0.04s
Settling Time	0.19s
Steady State Error	2.22e-14 %

The controlled system was also implemented in MATLAB/Simulink with controller parameters  $k_i$  and  $k_p$  calculated as 14.12 and 0.489 respectively. The speed performance of this controlled Induction motor is plotted in Figure 12.

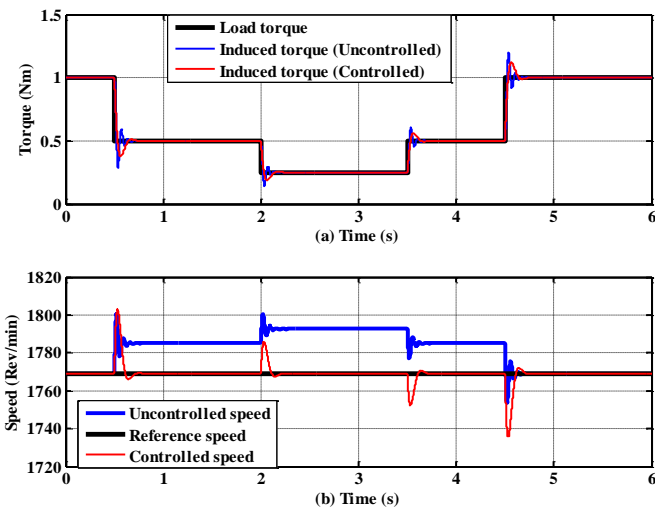


Fig. 12 (a): Torque performances (b): Speed performances of the uncontrolled and controlled three-phase induction motor

Given same load disturbances at the same simulation times as before, it can be observed in Figure 12 (a) that, although the induced torque response of the controlled motor undergoes some transient, the oscillations are significantly reduced. The speed of the controlled system in Figure 12(b), on the other hand, rises or falls sharply depending on whether the load torque is reduced or increased at the instant of the disturbances but tracks the commanded or reference speed and returns to its initial

(i.e., rated) value of 1770 rev/min. It maintains this value till end of simulation time despite the changes in load torque. Oscillations in speed have reduced significantly as well and this reduction can be observed in Figure 12 (b). There is an overshoot and a slight undershoot in the value of motor speed following the disturbances. These results validate the prediction from the step response plot of Figure 11.

## 6 CONCLUSION

The speed and torque responses of an un-controlled and controlled three phase induction motor were examined and discussed. The  $d-q$  reference frame model of the three-phase induction motor was presented and modified to allow for an independent control of torque and flux in the motor. A PI controller was designed in the light of classical control theory and analytical expressions were obtained for controller parameters  $k_i$  and  $k_p$ . In carrying out the controller design, the chosen cross-over frequency was imposed at a desired phase margin that produces a stable system. The crossover frequency was selected as 50 rad/s so as to obtain a very fast speed response and a phase margin of  $60^\circ$  was chosen for a stable closed loop operation. The parameters  $k_i$  and  $k_p$  of the PI controller were determined analytically from two closed form equations derived from the imposition of the chosen cross-over frequency at the desired phase margin that makes for a stable closed loop. A step response of the controlled motor was obtained and characterized.

A significant change in speed of the uncontrolled motor was observed when the motor was subjected to load disturbances in contrast to that of the controlled motor which returned quickly to its initial value after similar disturbances, thereby validating the prediction from the step response. The results obtained demonstrate the effectiveness and applicability of the controller design suggested in this paper. Going forward, a prototype model will be built with a view to verifying, experimentally, the simulation results obtained in this work. A robust controller design may be explored for further work as well. The controlled speed response will invariably lead to high efficiency and good precision in applications where it is deployed.

## REFERENCES

Abad, G. (2017). Power Electronics and Electric Drives for Traction Applications. John Wiley & Sons, United Kingdom.

Alahmad, A. and Kaçar, F. (2021). Simulation of Induction Motor Driving by Bridge Inverter at  $120^\circ$ ,  $150^\circ$ , and  $180^\circ$  Operation. *8th International Conference on Electrical and Electronics Engineering (ICEEE)*, pp. 121-125. Doi: 10.1109/ICEEE52452.2021.9415930.

Biswal, P. and Satpathy, S. (2021). Vector Control of 3-Phase Induction Motor. *1st Odisha International Conference on Electrical Power Engineering, Communication and Computing Technology (ODICON)*, pp. 1-4. Doi: 10.1109/ODICON50556.2021.9428930

El-Zohri, E. H. and Mosbah, M. A. (2019). Comparative Evaluation of PWM Techniques Used at Mega 328/p with PI Control for Inverter-Fed Induction Motor. *Proceedings of the International Conference on Innovative Trends in Computer Engineering (ITCE)*, Aswan, Egypt, pp. 219-224.

Hareesh, A. and Jayanand, B. 2021. Scalar and Vector Controlled Infinite Level Inverter (ILI) Topology Fed Open-Ended Three-Phase Induction Motor. *IEEE Access*. 9: 98433-98459.

- Jafari, H., Hassanifar, M., Nazarpour, D. and Golshannavaz, S. (2021). A New Hybrid Three-Phase Multilevel Inverter Devoted to Electric Drive with Constant Volt per Hertz Control. *12th Power Electronics, Drive Systems, and Technologies Conference (PEDSTC)*, pp. 1-6. Doi: 10.1109/PEDSTC52094.2021.9405935.
- Ke, C., Wei, G., Weiwei, G., Wentao, W. and Zhaowen, H. (2020). Low Constant Speed Control of Heavy Haul Electric Locomotives Based on Variable Parameter PI Regulator. *IEEE Vehicle Power and Propulsion Conference*, Gijon, Spain, pp. 1-5.
- Kousalya, V. and Singh, B. (2021). Single Current Sensor-Based Vector Control of Solar PV-Battery Assisted Induction Motor Drive for Electric Vehicle. *3rd International Conference on Energy, Power and Environment: Towards Clean Energy Technologies*. pp. 1-6. Doi: 10.1109/ICEPE50861.2021.9404532
- Krause, P. C., Wasynczuk, O., Sudhoff, S. D. and Pekarek, S. (2013). Analysis of electric machinery and drive systems. U.S.A, John Wiley & Sons
- Li, Z., Xia, J., Guo, Y. and Zhang, X. (2021). Fault-Tolerant Predictive Torque Control Design for Induction Motor Drives Based on Discrete Space Vector Modulation. *IEEE Journal of Emerging and Selected Topics in Power Electronics*. 9(5): 5441-5451. Doi: 10.1109/JESTPE.2021.3064979.
- Lim, Y., Lee, J. and Lee, K. (2019). Advanced Speed Control for a Five-Leg Inverter Driving a Dual-Induction Motor System. *IEEE Transactions on Industrial Electronics*, 66(1): 707-716.
- Magagula, G. S., Nnachi, A. F. and Akumu, A. O. (2020). Broken Rotor Bar Fault Simulation and Analysis in d-q Reference Frame. *IEEE PES/IAS Power Africa*, pp. 1-4, Doi: 10.1109/PowerAfrica49420.2020.9219892.
- Metwaly, M. K., Azazi, H. Z., Deraz, S. A., Dessouki, M. E. and Zaky, M. S. (2019). Power Factor Correction of Three-Phase PWM AC Chopper Fed Induction Motor Drive System using HBCC Technique. *IEEE Access*. 7: 43438-43452.
- Mohan, N. (2014). Advanced electric drives: analysis, control, and modeling using /Simulink. Hoboken, New Jersey, John Wiley & Sons.
- Richardson, M. T., Patterson, V. and Parchment, A. (2021). Microcontroller Based Space Vector Pulse Width Modulation Speed Control of Three-phase Induction Motor. *SoutheastCon*, pp. 1-6, Doi: 10.1109/SoutheastCon45413.2021.9401922.
- Sahu, A., Mohanty, K. A. and Mishra, R. N. (2021). Design of MPC-PSO based Torque Regulator for DTC-SVM Induction Motor Drive. *1st International Conference on Power Electronics and Energy (ICPEE)*, pp. 1-6. Doi: 10.1109/ICPEE50452.2021.9358559.
- Samudera, S. H., Rifadil, M. M., Ferdiansyah, I., Nugrahas, D., Qudsi, O.A. and Purwanto, E. (2020). Three Phase Induction Motor Dynamic Speed Regulation using IP Controller. *Proceedings of the 3rd International Seminar on Research of Information Technology and Intelligent Systems*, pp. 406 – 411.
- Sharma, G., Parashar, D. and Chandel, A. (2020). Analysis of Dynamic Model of Three Phase Induction Motor with MATLAB/SIMULINK. *International Conference on Advances in Computing, Communication & Materials (ICACCM)*, Dehradun, India, pp. 51-58. IEEE.
- Umar, M. F., Akbar, M. N. and Kazmi, S. M. R. (2018). Design and Simulation of a 3 Phase Induction Motor Drive based on Indirect Rotor Field Orientation using MATLAB Simulink Tool. *1st International Conference on Power, Energy and Smart Grid (ICPESG)*, pp. 1-6, Doi: 10.1109/ICPESG.2018.8384497.
- Zand, M., Nasab, M. A., Khoobani, M., Jahangiri, A., and Kimiai, A. H. (2021). Robust Speed Control for Induction Motor Drives Using STSM Control. *12th Power Electronics, Drive Systems, and Technologies Conference (PEDSTC)*, pp. 1-6. Doi: 10.1109/PEDSTC52094.2021.9405912.